Applied Mathematics and Computation 216 (2010) 1453–1468

Contents lists available at ScienceDirect

Applied Mathematics and Computation

journal homepage: www.elsevier.com/locate/amc

Image solutions for boundary value problems without sources

Jeng-Tzong Chen [a,b,*], Hung-Chih Shieh [a], Ying-Te Lee [a], Jia-Wei Lee [a]

[a] Department of Harbor and River Engineering, National Taiwan Ocean University, Keelung 20224, Taiwan
[b] Department of Mechanical and Mechatronic Engineering, National Taiwan Ocean University, Keelung 20224, Taiwan

ARTICLE INFO

Keywords:
Image method
Boundary value problem
Bipolar coordinates
Method of fundamental solution

ABSTRACT

In this paper, we employ the image method to solve boundary value problems in domains containing circular or spherical shaped boundaries free of sources. two and threeD problems as well as symmetric and anti-symmetric cases are considered. By treating the image method as a special case of method of fundamental solutions, only at most four unknown strengths, distributed at the center, two locations of frozen images and one free constant, need to be determined. Besides, the optimal locations of sources are determined. For the symmetric and anti-symmetric cases, only two coefficients are required to match the two boundary conditions. The convergence rate versus number of image group is numerically performed. The differences of the image solutions between 2D and 3D problems are addressed. It is found that the 2D solution in terms of the bipolar coordinates is mathematically equivalent to that of the simplest MFS with only two sources and one free constant. Finally, several examples are demonstrated to see the validity of the image method for boundary value problems.

1. Introduction

The image method is a popular approach in the theoretical physics [1] and has commonly been used in multidisciplines such as electro-magnetics, acoustics and optics. When solving problems by using the Green's functions for a bounded domain, the reflection is described by one or successive image sources, and the position and sign of the image sources is chosen so that the boundary conditions can be satisfied [2]. Green's function for a part of domain bounded by planes, circles or spherical surface in terms of the corresponding fundamental solution in the full space can be found in the literature [3]. In certain cases, it is possible to obtain the exact solution for a concentrated source in a domain through superimposing the infinite plane or infinite space solution for the given source and its image sources. Although the scope of this method is limited for special geometry, it yields a great deal of insight into the solution when it works [4,5]. As a result of the aforementioned consideration, many theoretical studies concerning the Green's function in circular and spherical boundaries have appeared in the literature. For example, Green's function for plane boundaries has been investigated [6]. The image method was employed to solve edge dislocation in an anisotropic film-substrate system [7] and dielectric plate [8]. Chen et al. [9,10] solved Green's functions of annulus or concentric spheres by using the image method. It is found that almost all the related works on the image method deal with the problem with a true source in the domain. Although Cheng's book [11] has employed the image method to solve the boundary value problems (BVPs) of an infinite space with two spherical boundaries, the frozen image locations were not found to be the focuses of the bispherical coordinates. However, we may wonder whether the image method may work for BVPs without sources in the domain. Bispherical and bipolar coordinates

* Corresponding author. Address: Department of Harbor and River Engineering, National Taiwan Ocean University, Keelung 20224, Taiwan.
E-mail address: jtchen@mail.ntou.edu.tw (J.-T. Chen).
URL: http://ind.ntou.edu.tw/~msvlab (J.-T. Chen).

0096-3003/$ - see front matter © 2010 Elsevier Inc. All rights reserved.
doi:10.1016/j.amc.2010.02.048

were always used to derive the analytical solutions for problems containing boundaries of two spheres or circles [12], respectively. The BVPs of eccentric annulus were solved in a unified way of conformal mapping [13]. Problems with several circular boundaries were solved by using the null-field BIEM [14].

In this paper, we will illustrate several examples to demonstrate the possible use of image method in solving 2D and 3D BVPs without sources. Symmetric, anti-symmetric and eccentric cases are considered. Based on the singularities distributed outside the domain for the image method, it can be seen as a special method of fundamental solutions (MFS) with optimal locations and strengths of sources. To verify our image idea, analytical solutions by using the bipolar and bispherical coordinates are used to check the accuracy of our results. Besides, numerical results using the conventional MFS and null-field BIEM are also given for comparison. An infinite space with two spherical cavities as well as an infinite plane with two circular holes are both considered. Besides, an eccentric sphere is also given. Also, the static result for a limiting case of two-spheres radiation to simulate Laplace problems is provided for comparison.

2. Derivation of the image solution for BVPs

2.1. 3D BVP

The problem of an infinite space with two spherical cavities is shown in Fig. 1(a) and the governing equation is

$$\nabla^2 u(x) = 0, \quad x \in D, \tag{1}$$

where ∇^2 is the Laplacian, $u(x)$ is the potential function and D is the domain of interest. For a two-spheres case, the boundary conditions are

$$u(x) = V_1, \quad x \in B_1, \tag{2}$$

$$u(x) = V_2, \quad x \in B_2, \tag{3}$$

where B_1 and B_2 are left and right spherical boundaries with constant boundary data of V_1 and V_2, respectively. In this case, the analytical solution [12] was derived in terms of the bispherical coordinates as shown below:

$$u(\xi,\eta) = \sqrt{2\cosh\eta - 2\cos\xi}\sum_{n=0}^{\infty}\left[\left(\frac{V_2+V_1}{2}\right)\frac{\cosh\left(n+\frac{1}{2}\right)\eta}{\cosh\left(n+\frac{1}{2}\right)\eta_0} + \left(\frac{V_2-V_1}{2}\right)\frac{\sinh\left(n+\frac{1}{2}\right)\eta}{\sinh\left(n+\frac{1}{2}\right)\eta_0}\right]e^{-(n+1/2)\eta_0}P_n(\cos\xi), \tag{4}$$

where ξ = constant is a family of spindle-shaped surfaces passing through the poles $(0,\pm c,0)$, η_0 is on the right spherical boundary, η =constant shows a surface of $\ln(r_{c1}/r_{c2})$ = constant, and $P_n(\bullet)$ is the Legendre polynomial. It contains both symmetric and anti-symmetric problems.

The problem of infinite space with two spherical cavities can be seen as a combination of symmetric and anti-symmetric problems as shown in Fig. 1(b) and (c). The fundamental solution of the 3D Laplace equation is shown below:

$$U(x,s) = \frac{-1}{r}, \tag{5}$$

where r is the distance between the source point s and the field point $x(r \equiv |x-s|)$. For the symmetric case, we derive the solution by using the image concept. To satisfy the nonhomogeneous boundary conditions (BCs) on the two spherical surfaces, both artificial sources at the two centers outside the domain are initiated in advance. However, the source at the left (right) center also results a nonzero potential on the right (left) boundary. Therefore, successive images are required to construct the solution as given below:

$$u(x) = \lim_{N\to\infty}\left\{q^s(N)\left[\left(\frac{1}{r_{o1}}+\frac{1}{r_{o2}}\right)+\sum_{i=1}^{N}\left(\frac{-w_{4i-3}}{|x-s_{4i-3}|}-\frac{w_{4i-2}}{|x-s_{4i-2}|}+\frac{w_{4i-1}}{|x-s_{4i-1}|}+\frac{w_{4i}}{|x-s_{4i}|}\right)\right]+\frac{c_1^s(N)}{|x-s_{c_1}|}+\frac{c_2^s(N)}{|x-s_{c_2}|}\right\}, \tag{6}$$

where three coefficients of symmetric case, $q^s(N), c_1^s(N)$ and $c_2^s(N)$ are required to be determined by matching the boundary conditions, r_{o1} and r_{o2} are the distances between center and field point. Two frozen images, s_{c1} and s_{c2}, are found after successive images. The locations of two frozen images must simultaneously satisfy

$$\frac{d}{2}+R_{c2} = \frac{a^2}{\left(\frac{d}{2}-R_{c1}\right)}, \quad R_{c1} = R_{c2}, \tag{7}$$

where a, d, R_{c1} and R_{c2} are shown in Fig. 2. The distance between the two focuses is denoted by

$$|R_{c1}+R_{c2}| = 2c. \tag{8}$$

The parameter c is the half distance between the two focuses in the bispherical coordinates which can be obtained by:

$$c = \frac{\sqrt{d^2-4a^2}}{2}. \tag{9}$$

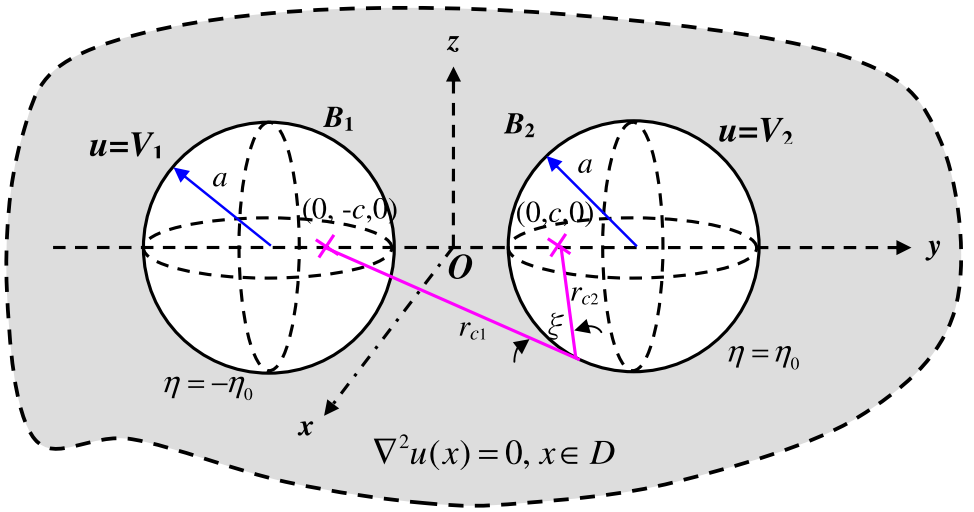

(a) An infinite space problem

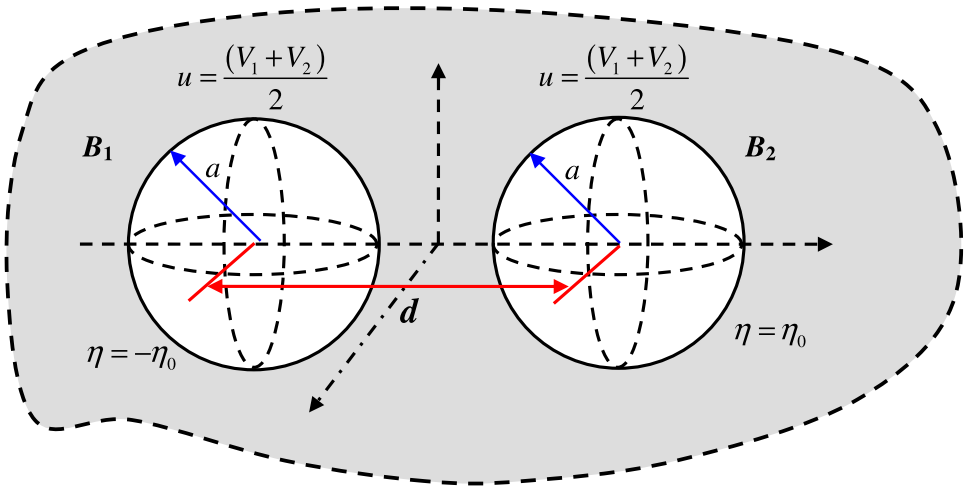

(b) symmetric problem

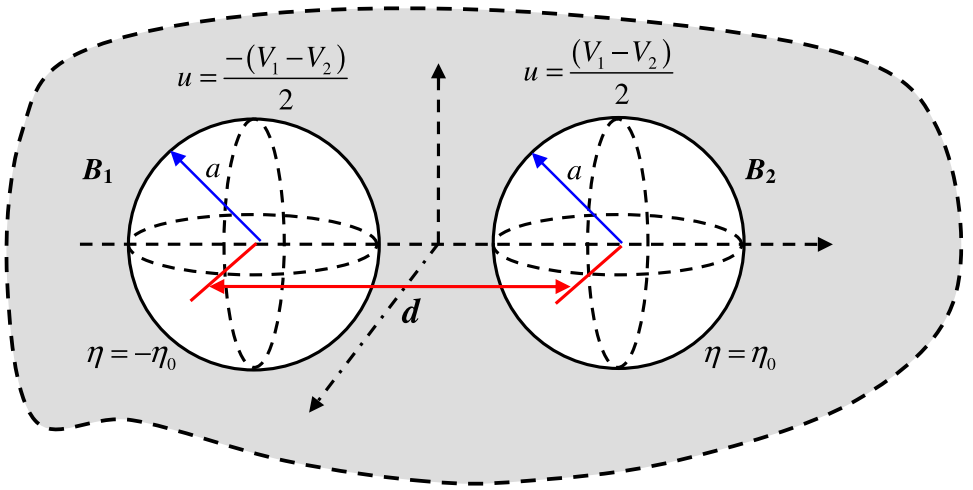

(c) anti-symmetric problem

Fig. 1. (a) An infinite space problem with two spherical cavities composed of: (b) symmetric problem and (c) anti-symmetric problem.

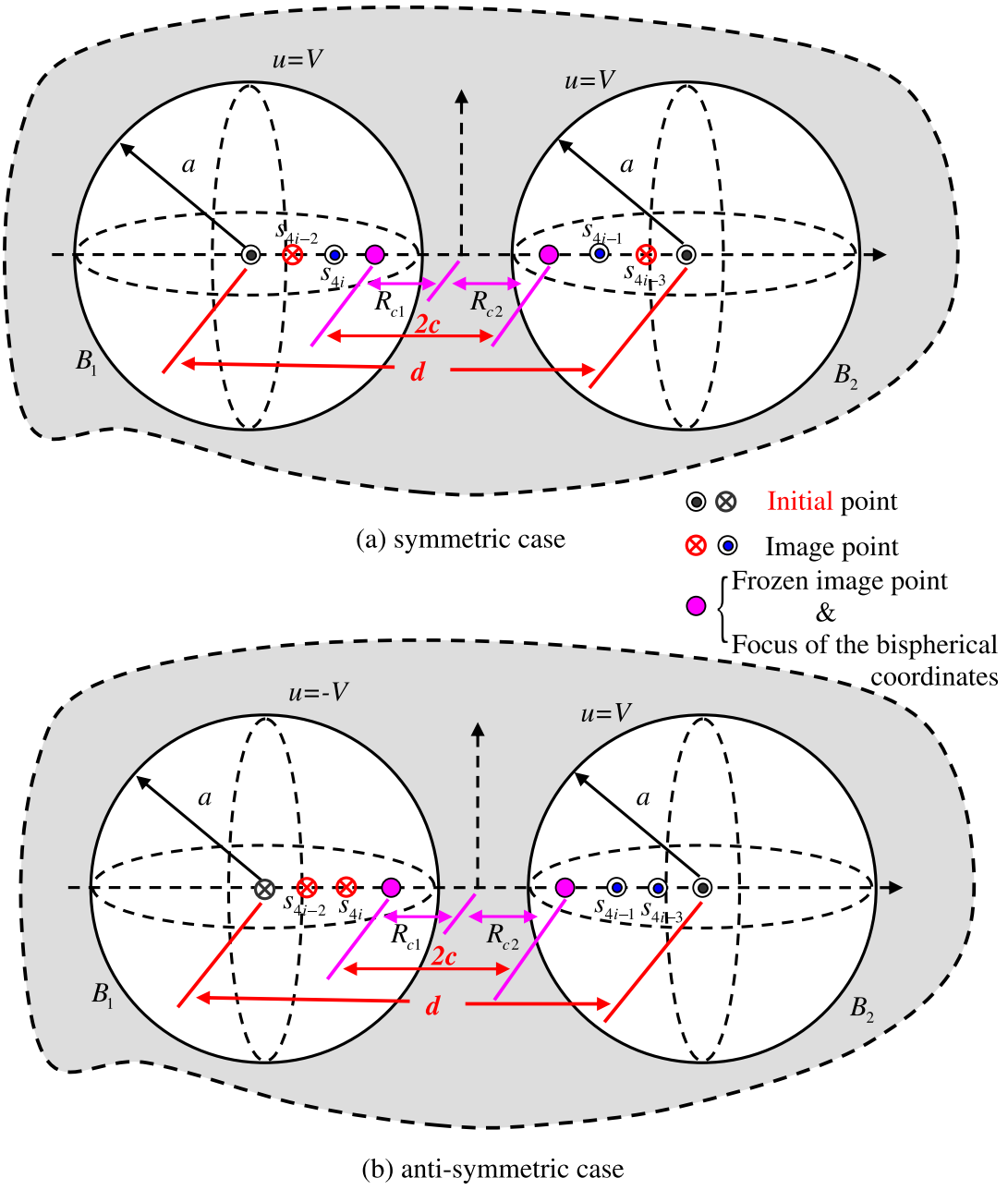

Fig. 2. Successive images for the: (a) symmetric and (b) anti-symmetric cases.

The w_k in Eq. (6) is the weighting of the kth image source that can be obtained by using the formula of image location [9,10] as shown below:

$$
\begin{aligned}
&w_1 = \frac{a}{d}, \quad w_5 = \frac{aw_4}{d - R_4}, \ldots, w_{4i-3} = \frac{aw_{4i-4}}{d - R_{4i-4}}, \\
&w_2 = \frac{a}{d}, \quad w_6 = \frac{aw_3}{R_3}, \ldots, w_{4i-2} = \frac{aw_{4i-5}}{R_{4i-5}}, \\
&w_3 = \frac{aw_2}{d - R_2}, \quad w_7 = \frac{aw_6}{d - R_6}, \ldots, w_{4i-1} = \frac{aw_{4i-2}}{d - R_{4i-2}}, \\
&w_4 = \frac{aw_1}{R_1}, \quad w_8 = \frac{aw_5}{R_5}, \ldots, w_{4i} = \frac{aw_{4i-3}}{R_{4i-3}}, \quad i = 2, 3, \ldots, \infty,
\end{aligned}
\tag{10}
$$

where R_k is the distance between the kth image source and the center of left cavity, and they are determined by the recurrence relation

$$\begin{aligned}
&R_1 = d - \frac{a^2}{d}, \quad R_5 = d - \frac{a^2}{d - R_4}, \ldots, R_{4i-3} = d - \frac{a^2}{d - R_{4i-4}}, \\
&R_2 = \frac{a^2}{d}, \quad R_6 = \frac{a^2}{R_3}, \ldots, R_{4i-2} = \frac{a^2}{R_{4i-5}}, \\
&R_3 = d - \frac{a^2}{d - R_2}, \quad R_7 = d - \frac{a^2}{d - R_6}, \ldots, R_{4i-1} = d - \frac{a^2}{d - R_{4i-2}}, \\
&R_4 = \frac{a^2}{R_1}, \quad R_8 = \frac{a^2}{R_5}, \ldots, R_{4i} = \frac{a^2}{R_{4i-3}}, \quad i = 2, 3, \ldots, \infty.
\end{aligned} \tag{11}$$

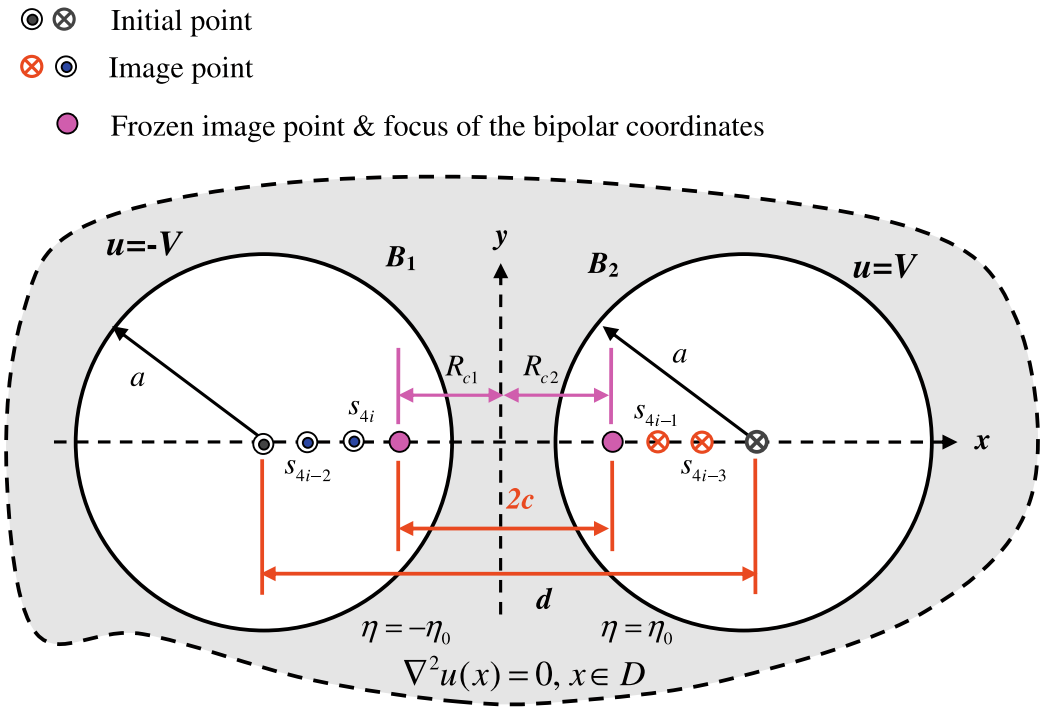

Fig. 3. Images locations for the 2D anti-symmetric case.

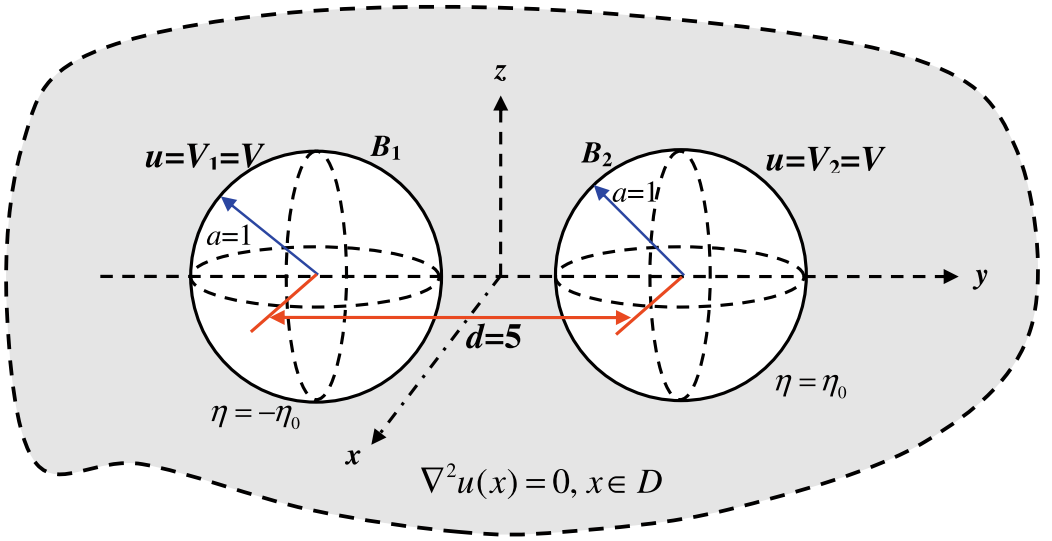

Fig. 4. Problem sketch for the 3D symmetric problem.

Here, the image solution for an anti-symmetric problem is shown below:

$$u(x)=\lim_{N\to\infty}\left\{q^a(N)\left[\left(\frac{-1}{r_{o1}}+\frac{1}{r_{o2}}\right)+\sum_{i=1}^{N}\left(\frac{-w_{4i-3}}{|x-s_{4i-3}|}+\frac{w_{4i-2}}{|x-s_{4i-2}|}-\frac{w_{4i-1}}{|x-s_{4i-1}|}+\frac{w_{4i}}{|x-s_{4i}|}\right)\right]+\frac{c_1^a(N)}{|x-s_{c_1}|}+\frac{c_2^a(N)}{|x-s_{c_2}|}\right\}, \tag{12}$$

where the coefficients of the anti-symmetric case, $q^a(N), c_1^a(N)$ and $c_2^a(N)$, are required to be determined by matching the boundary conditions, $q^s(N)$ and $q^a(N)$ are the initial strengths for symmetric and anti-symmetric cases, respectively, which can be determined later by matching the boundary conditions. Successive images for the symmetric and anti-symmetric cases were shown in Fig. 2.

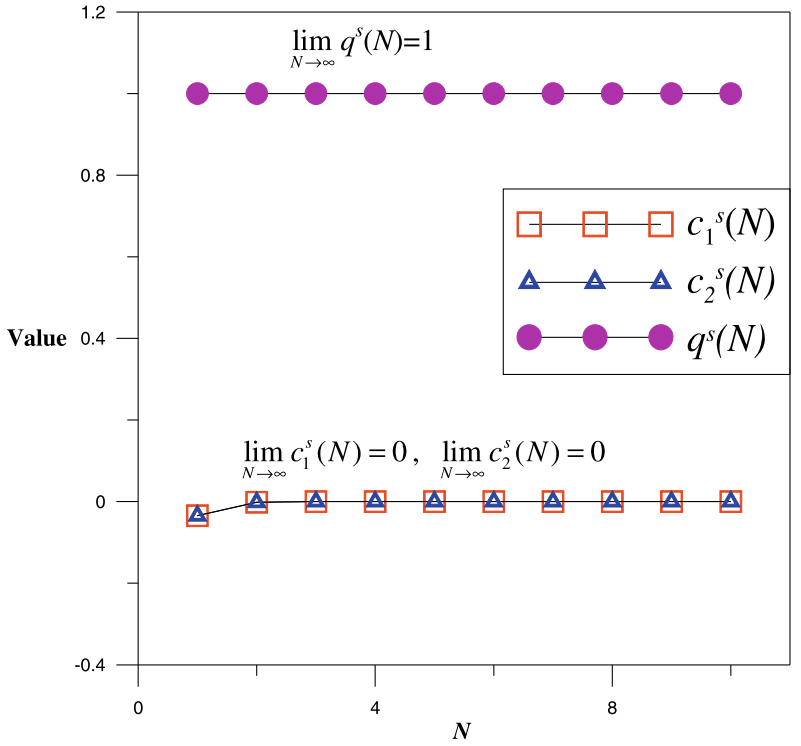

Fig. 5. Coefficients of $q^s(N), c_1^s(N)$ and $c_2^s(N)$ versus N for an infinite space with two spherical cavities subject to the symmetric boundary condition.

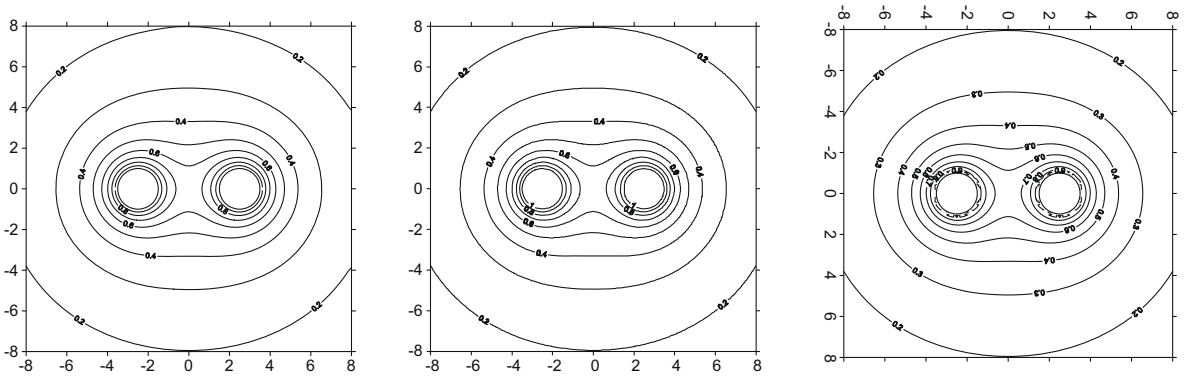

Fig. 6. Potential contours: (a) an image solution, (b) an analytical solution using the bispherical coordinates and (c) a limiting case of static solution using the null-field BIEM [15] (x–y plane).

2.2. 2D BVP

Let us consider an infinite plane with two circular holes subject to the anti-symmetric boundary condition. Similarly, the 2D anti-symmetric problem is solved by using the image method in a similar way of 3D case. The fundamental solution of the 2D Laplace equation is given below:

$$U(x,s) = \ln(r). \tag{13}$$

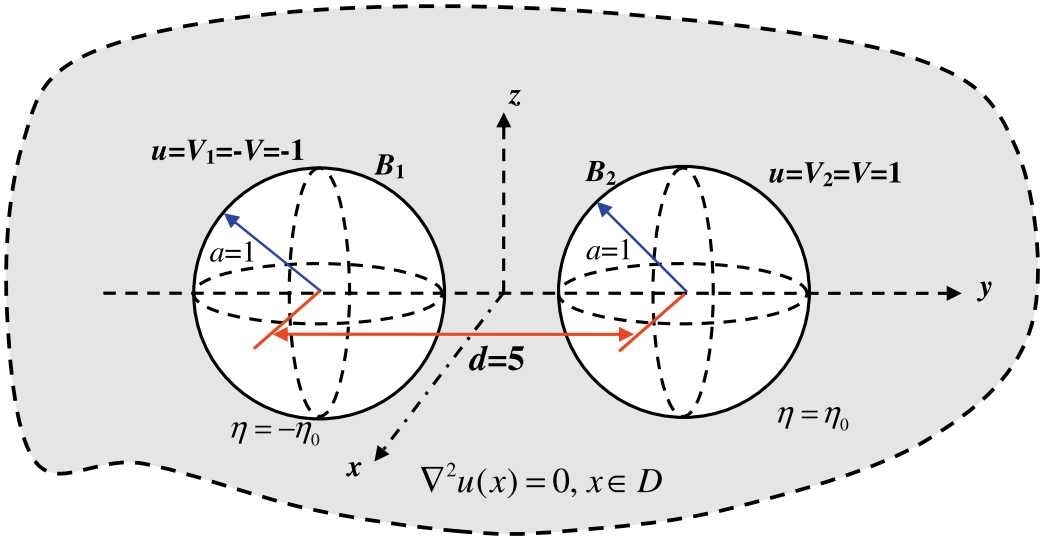

Fig. 7. Problem sketch for the 3D anti-symmetric problem.

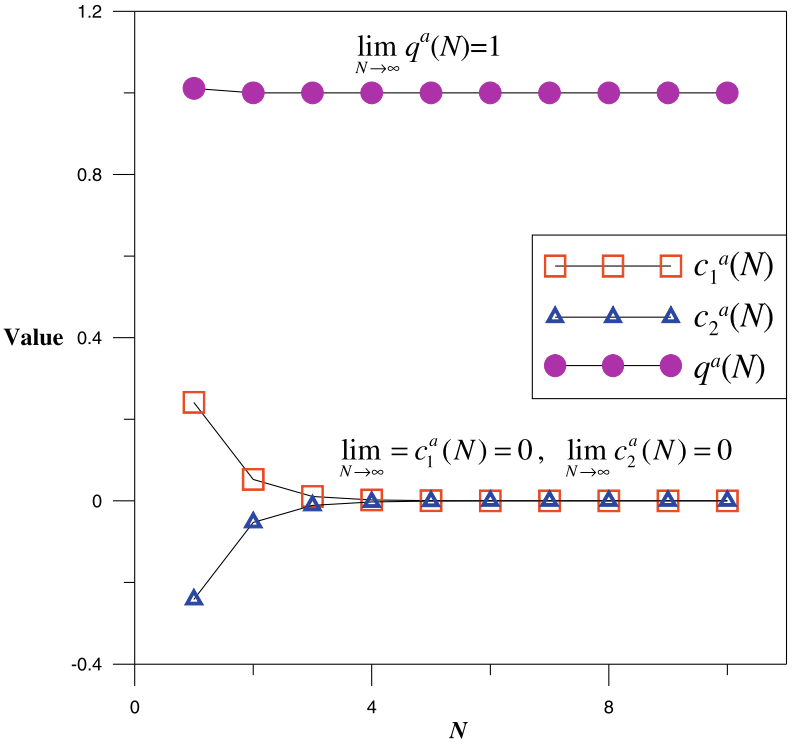

Fig. 8. Coefficients of $q^a(N), c_1^a(N)$ and $c_2^a(N)$ versus N for an infinite space with two spherical cavities subject to the anti-symmetry boundary condition.

For the anti-symmetric case, the boundary conditions are

$$u(x) = V_1 = -V, \quad x \in B_1, \tag{14}$$

$$u(x) = V_2 = V, \quad x \in B_2, \tag{15}$$

where B_1 and B_2 are left and right circular boundaries with boundary data of V_1 and V_2, respectively. Therefore, the image solution for the 2D anti-symmetric problem in Fig. 3 can be constructed as

$$u(x) = \lim_{N\to\infty} \left\{ q(N) \left[(-\ln r_{o1} + \ln r_{o2}) + \sum_{i=1}^{N} (\ln|x - s_{4i-3}| - \ln|x - s_{4i-2}| + \ln|x - s_{4i-1}| - \ln|x - s_{4i}|) \right] + c_1(N) \ln|x - s_{c_1}| + c_2(N) \ln|x - s_{c_2}| + e(N) \right\}, \tag{16}$$

where $q(N)$ is an initial strength at the two centers of circular hole which can be determined later by matching the boundary conditions, s_{c1} and s_{c2} are two locations of final two frozen images which are similar to the 3D case, $c_1(N)$ and $c_2(N)$ are their corresponding strengths, $e(N)$ is the rigid body term, the iterative images and their locations are shown in Fig. 3. The exact solution [12] in terms of the bipolar coordinates is given below:

$$u(\xi, \eta) = \frac{V}{\ln|r_1/r_2|}\eta = \frac{V}{\eta_0}\eta. \tag{17}$$

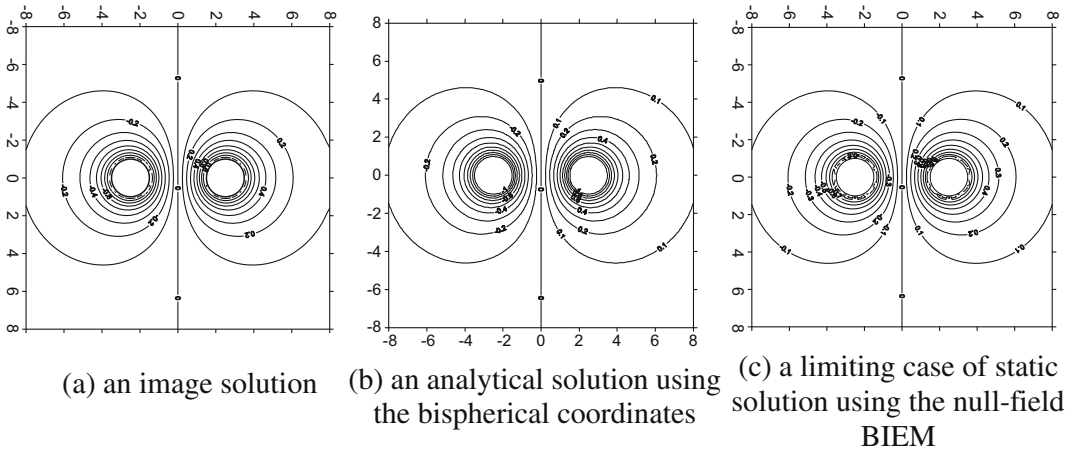

(a) an image solution (b) an analytical solution using the bispherical coordinates (c) a limiting case of static solution using the null-field BIEM

Fig. 9. Potential contours: (a) an image solution, (b) an analytical solution using the bispherical coordinates and (c) a limiting case of static solution using the null-field BIEM [15] (x–y plane).

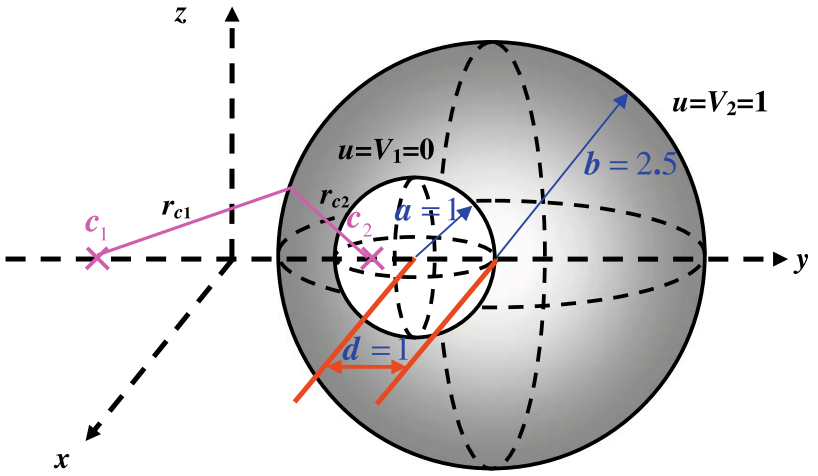

Fig. 10. Sketch for the problem of non-concentric spheres.

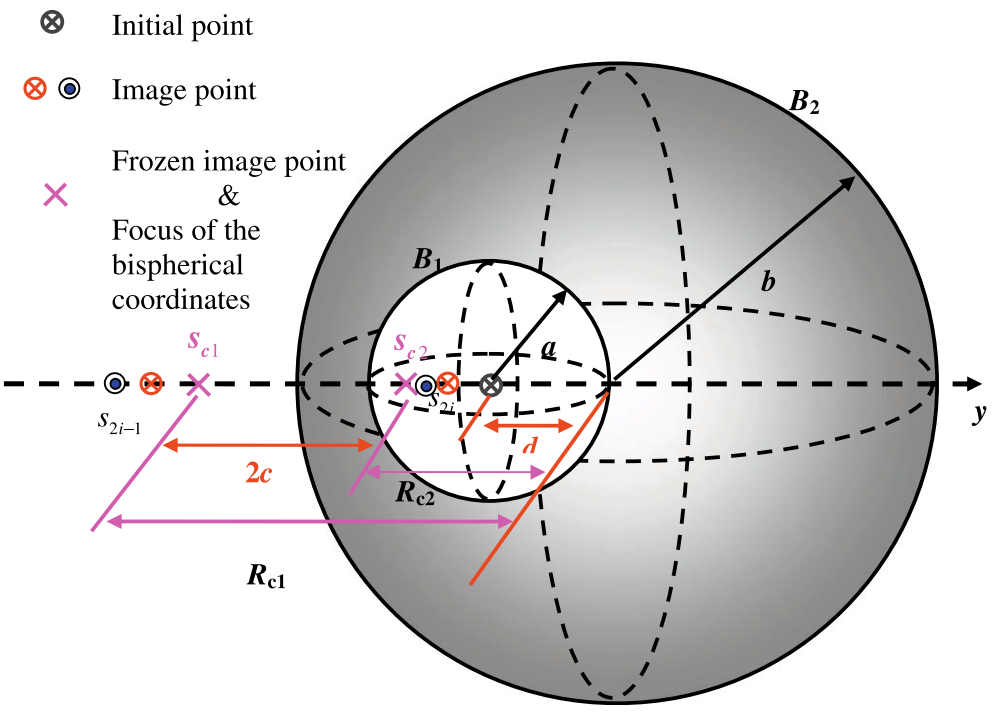

Fig. 11. Image location for the problem of the non-concentric spheres.

3. Illustrative examples and discussions

3.1. 3D problems

Case 1: an infinite space with two spherical cavities subject to symmetric boundary conditions (symmetric problem of $V_1 = V_2 = V = 1$

In the first case, the problem sketch for an infinite space with two spherical cavities is shown in Fig. 4. The centers of two cavities are set at (0, −2.5, 0) and (0, 2.5, 0), and the radii are both 1. By matching the boundary conditions, the analytical solution [12] can be simplified by using Eq. (4) as given below:

$$u(\xi,\eta) = \sqrt{2\cosh\eta - 2\cos\xi}\sum_{n=0}^{\infty}\left[V\frac{\cosh\left(n+\frac{1}{2}\right)\eta}{\cosh\left(n+\frac{1}{2}\right)\eta_0}\right]e^{-(n+1/2)\eta_0}P_n(\cos\xi). \tag{18}$$

By matching the boundary conditions, all the unknown coefficients in Eqs. (4)–(6), $q^s(N), c_1^s(N)$ and $c_2^s(N)$, can be determined as shown in Fig. 5. In the numerical experiment, we found that the coefficient of $q^s(N)$ is equal to 1, since the 3D fundamental solution is $-1/r$ where r is the distance between s and x $(r \equiv |x-s|)$, $\lim_{N\to\infty} c_1^s(N) = 0$ and $\lim_{N\to\infty} c_2^s(N) = 0$. Finally, we can find that the final frozen image points terminate at the focuses of the bispherical coordinates. The contour plots by using Eq. (6) of the image method and Eq. (18) in terms of the bispherical coordinates are shown in Fig. 6. It can be observed that our results are compared well with the analytical solution. Also, the static result for limiting solution of two-spheres radiation by using the null-field BIEM [15] is provided for comparison. Good agreement is also made.

Case 2: an infinite space with two spherical cavities subject to anti-symmetric boundary conditions (anti-symmetric problem of $V_1 = -V = -1, V_2 = V = 1$)

Fig. 7 is a sketch of an infinite space with two spherical cavities subject to anti-symmetry boundary conditions instead of the above symmetric case. The geometry data are the same as the case 1 and the analytical solution is obtained as follows:

$$u(\xi,\eta) = \sqrt{2\cosh\eta - 2\cos\xi}\sum_{n=0}^{\infty}\left[V\frac{\sinh\left(n+\frac{1}{2}\right)\eta}{\sinh\left(n+\frac{1}{2}\right)\eta_0}\right]e^{-(n-1/2)\eta_0}P_n(\cos\xi). \tag{19}$$

In a similar way of finding the successive images for matching the boundary conditions, the solution can be obtained by using Eqs. (4)–(12). After locating boundary points to match the boundary conditions, all the unknown coefficients, $q^a(N), c_1^a(N)$ and $c_2^a(N)$, versus N can be determined as shown in Fig. 8. Similarly, we also found that the final frozen image

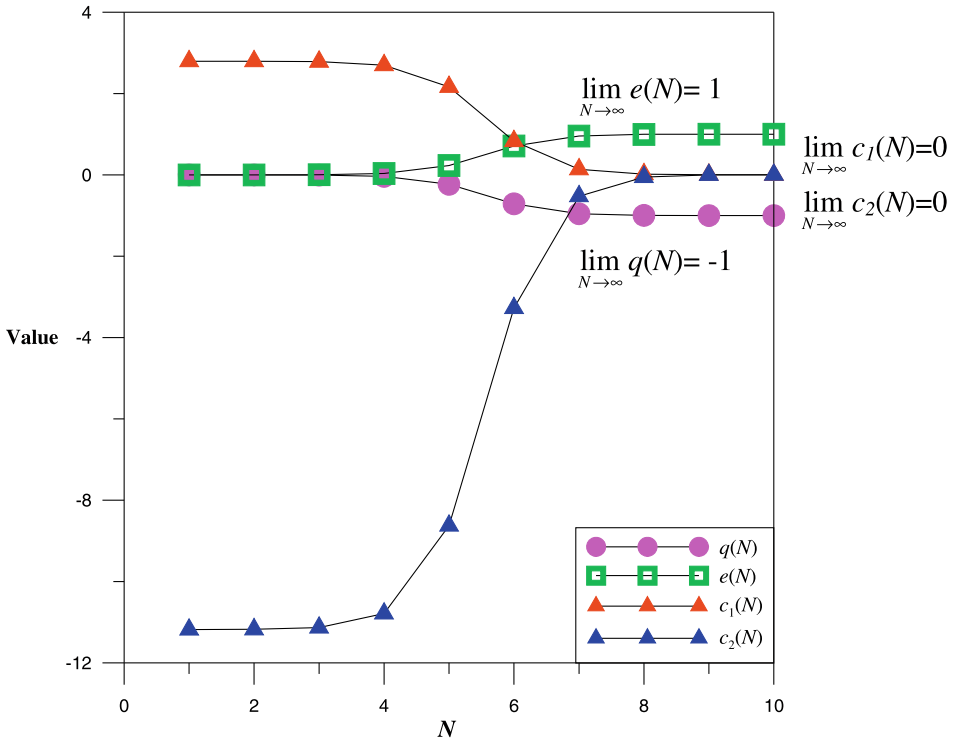

Fig. 12. Coefficients of $q(N), c_1(N), c_2(N)$ and $e(N)$ versus N for the non-concentric spherical problem.

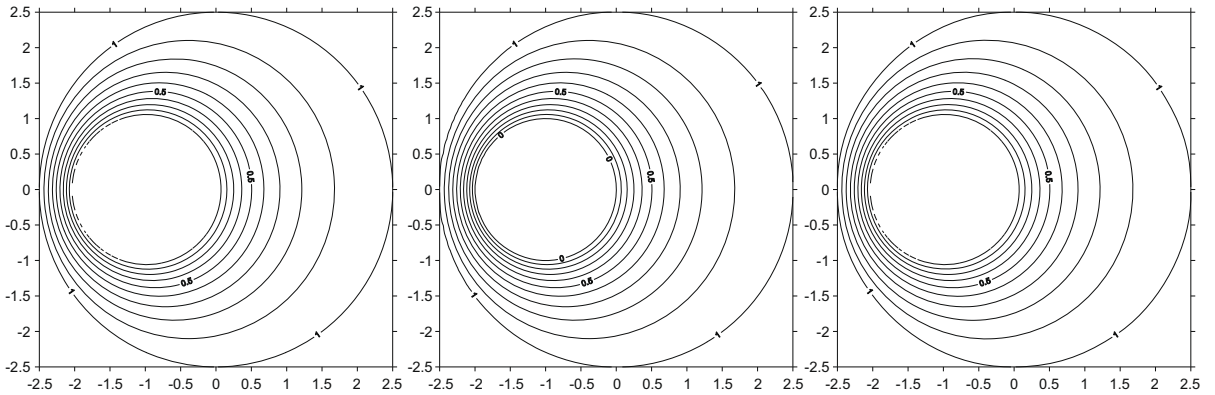

(a) an image solution (b) an analytical solution using the bispherical coordinates (c) a solution by using the MFS

Fig. 13. Potential contours: (a) an image solution, (b) an analytical solution using the bispherical coordinates [12] and (c) a solution by using the MFS (x-y plane).

points happen to be the focuses of the bispherical coordinates. The contour plots by using Eq. (12) in the image method and Eq. (19) of the analytical solution are shown in Fig. 9. The results of our approach are compared well with the analytical solution by using the bispherical coordinates. Also, the static result for limiting solution of two-spheres radiation using the null-field BIEM [15] is provided for comparison. Good agreement is also made.

Case 3: a non-concentric sphere ($V_1 = 0, V_2 = 1$)

In this case, the two radii of inner and outer spheres are $a = 1$ and $b = 2.5$, respectively. The distance d between the two centers is equal to 1 as shown in Fig. 10. After successive images, the image solution can be obtained as shown below:

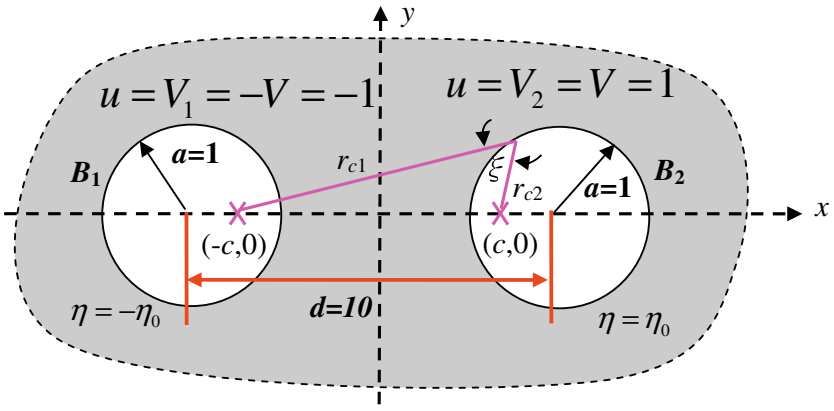

Fig. 14. An infinite plane with two circular holes in the bipolar coordinate system.

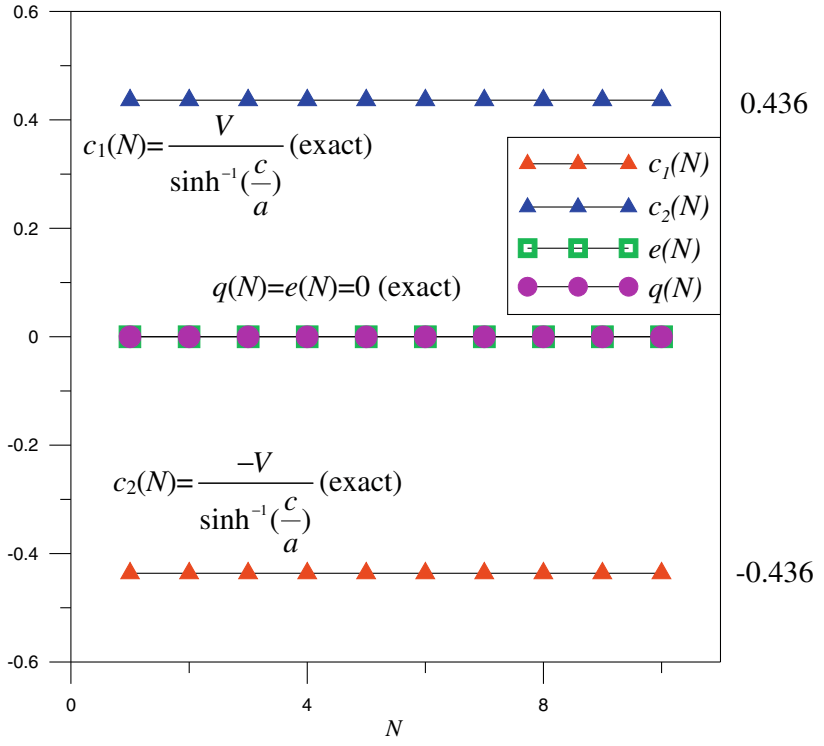

Fig. 15. Coefficients of $q(N), c_1(N), c_2(N)$ and $e(N)$ versus N for an infinite plane with two circular holes.

$$u(x) = \lim_{N\to\infty}\left\{q(N)\left[\frac{-1}{r} + \sum_{i=1}^{N}\left(\frac{-w_{2i-1}}{|x - s_{2i-1}|} + \frac{w_{2i}}{|x - s_{2i}|}\right)\right] + \frac{c_1(N)}{|x - s_{c_1}|} + \frac{c_2(N)}{|x - s_{c_2}|} + e(N)\right\}. \tag{20}$$

Since the center of outer sphere is in the domain, we only put an artificial source at the center of inner sphere to satisfy the governing equation. Similarly, two frozen images are found after successive images. The locations of two frozen images are governed by

$$R_{c1} = \frac{b^2}{R_{c2} - d} + d, \quad R_{c2} = \frac{a^2}{R_{c1}}, \tag{21}$$

where R_{c1} and R_{c2} are the y coordinates for the left and right focuses, respectively, as shown in Fig. 11. The distance between the two focuses is denoted by

$$|R_{c1} - R_{c2}| = 2c. \tag{22}$$

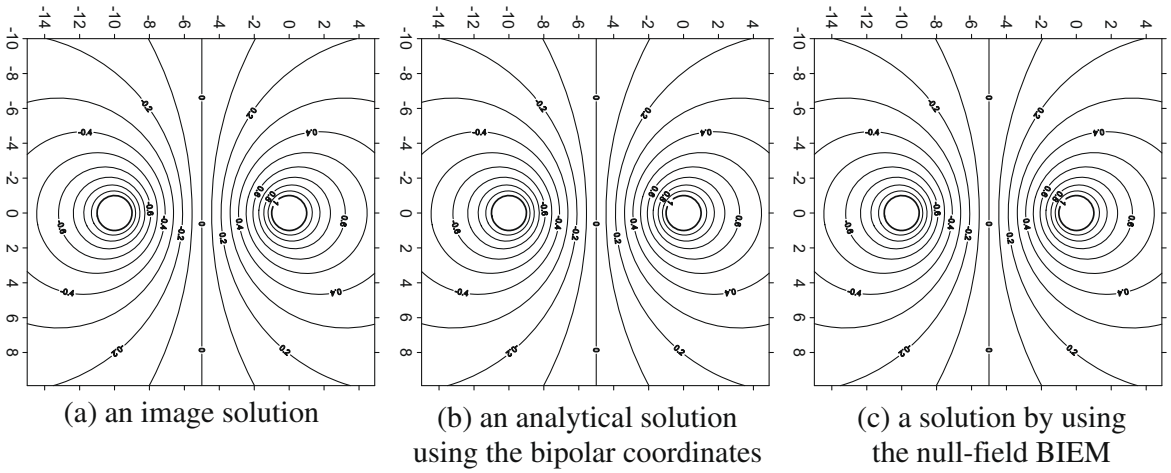

Fig. 16. Potential contours: (a) an image solution, (b) an analytical solution using the bipolar coordinates and (c) a solution by using the null-field BIEM [14].

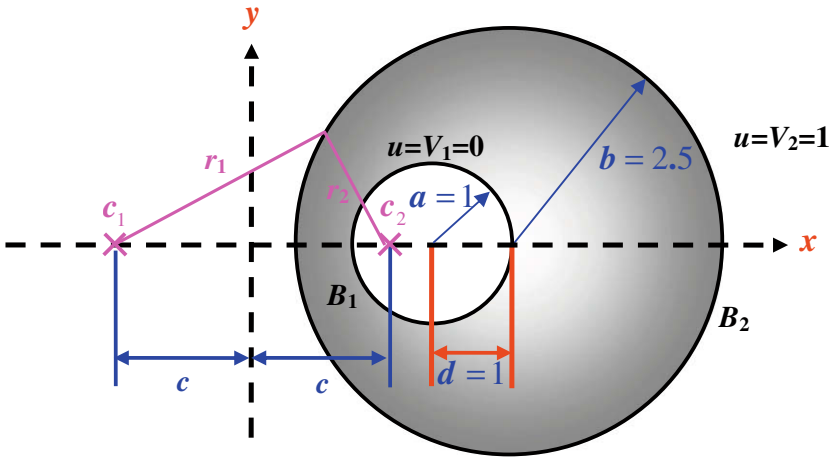

Fig. 17. Problem sketch for an eccentric annulus.

The parameter c is the half distance between two focuses in the bispherical coordinates which can be obtained by:

$$c = \frac{\sqrt{a^4 - 2a^2b^2 + b^4 - 2a^2d^2 - 2b^2d^2 + d^4}}{2d}. \tag{23}$$

After matching the boundary conditions, the unknown coefficients, $q(N), c_1(N), c_2(N)$ and $e(N)$, versus N are shown in Fig. 12. The frozen images happen to be the two focuses in the bispherical coordinates. The analytical solution obtained by using the bispherical coordinates is

$$u(\xi,\eta) = \sqrt{2\cosh\eta - 2\cos\xi}\sum_{n=0}^{\infty}\left[\frac{V_1(e^{2(n+1/2)\eta} - e^{2(n+1/2)\eta_2}) - V_2(e^{2(n+1/2)\eta} - e^{2(n+1/2)\eta_1})}{e^{2(n+1/2)\eta_1} - e^{2(n+1/2)\eta_2}}\right]e^{-(n+1/2)\eta}P_n(\cos\xi). \tag{24}$$

Fig. 13(a)–(c) show the potential contours by using the image method, the bispherical coordinates and the method of fundamental solutions, respectively. It is found that the results of three approaches match well with each other.

3.2. 2D problems

Case 4: an infinite plane with two circular holes subject to anti-symmetric BCs ($V_1 = -V = -1,\ V_2 = V = 1$)

It is interesting to find that $q(N)$ for 3D case can be obtained in advance to fit the boundary condition. We may wonder whether the $q(N)$ of the 2D problem can be determined in the same way as 3D case. The problem sketch for an infinite plane with two circular holes subject to anti-symmetric boundary conditions is shown in Fig. 14. The distance between the centers of two circular holes is 10, and the radii of two holes are both 1. The frozen images happen to be the two focuses in the

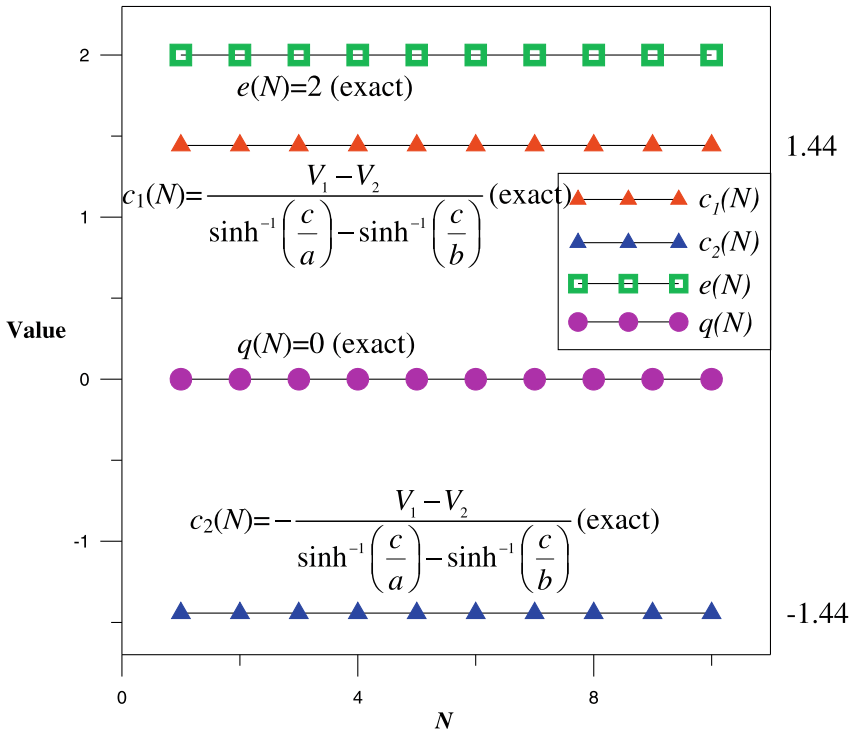

Fig. 18. Coefficients of $q(N), c_1(N), c_2(N)$ and $e(N)$ versus N for the eccentric annulus.

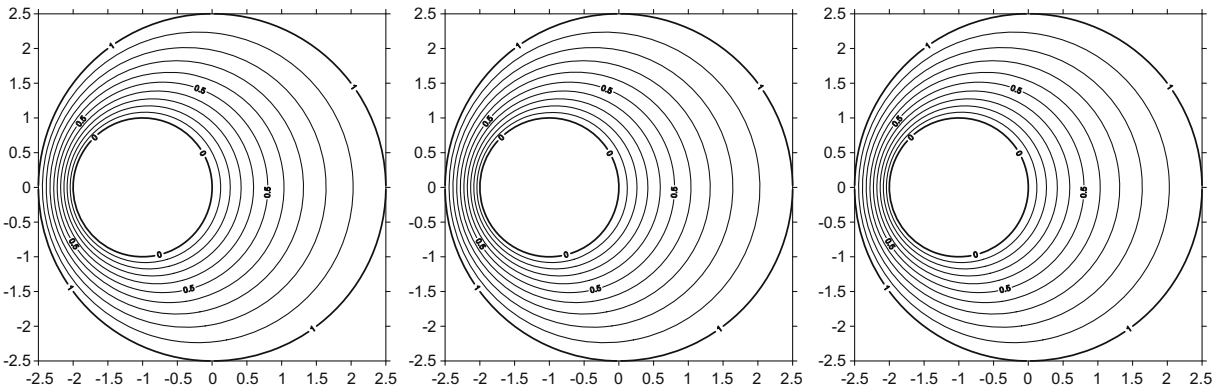

Fig. 19. Potential contours: (a) an image solution, (b) an analytical solution using the bipolar coordinates and (c) a solution by using the null-field BIEM [13].

bipolar coordinates. After matching the boundary conditions in Eqs. (14) and (15), the unknown coefficients of $q(N)$, $c_1(N), c_2(N)$ and $e(N)$ versus N are shown in Fig. 15. It is interesting to find that the strengths of $q(N)$ and $e(N)$ are zero. Besides, we also observe that $c_1(N) = -c_2(N)$ in numerical experiment and therefore the image solution of the anti-symmetrical case can be written as

$$u(x) = c_1(N)\left[\ln|x - s_{c_1}| - \ln|x - s_{c_2}|\right], \tag{25}$$

where the coefficient $c_1(N)$ is determined by matching the boundary condition $(u(x)|_{x\in B_2} = V = 1)$ as given below:

$$c_1(N) = \frac{V}{\ln|x - s_{c_1}| - \ln|x - s_{c_2}|}, \quad x \in B_2, \tag{26}$$

Table 1
Anti-symmetric problem of 2D and 3D.

Domain	2D problem	3D problem
Figure sketch	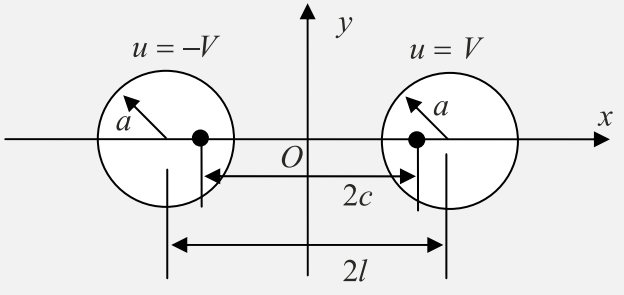	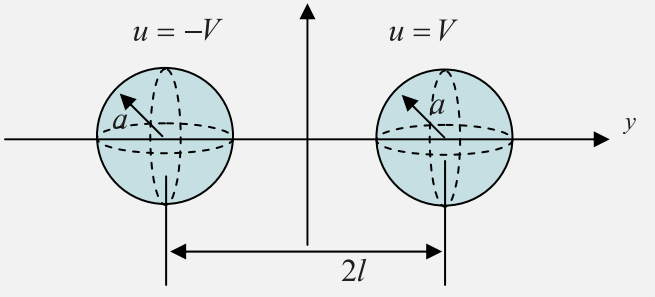
Image solution	$u(x)=\lim_{N\to\infty}\Big\{q(N)[(-\ln r_{o1}+\ln r_{o2})$ $+\sum_{i=1}^{N}(\ln\lvert x-s_{4i-3}\rvert-\ln\lvert x-s_{4i-2}\rvert+\ln\lvert x-s_{4i-1}\rvert-\ln\lvert x-s_{4i}\rvert)]$ $+c_1(N)\ln\lvert x-s_{c1}\rvert+c_2(N)\ln\lvert x-s_{c2}\rvert\Big\}$	$u(x)=\lim_{N\to\infty}\Big\{q^a(N)\Big[\Big(\frac{-1}{r_{o1}}+\frac{1}{r_{o2}}\Big)$ $+\sum_{i=1}^{N}\Big(\frac{-w_{4i-3}}{\lvert x-s_{4i-3}\rvert}+\frac{w_{4i-2}}{\lvert x-s_{4i-2}\rvert}-\frac{w_{4i-1}}{\lvert x-s_{4i-1}\rvert}+\frac{w_{4i}}{\lvert x-s_{4i}\rvert}\Big)\Big]+\frac{c_1^a(N)}{\lvert x-s_{c_1}\rvert}+\frac{c_2^a(N)}{\lvert x-s_{c_2}\rvert}\Big\}$
Value of coefficient	$q(N)=0$ $c_1(N)=c_2(N)\neq 0$ $c_1(N)=\frac{V}{\sinh^{-1}(\frac{c}{a})}, c_2(N)=\frac{-V}{\sinh^{-1}(\frac{c}{a})}$	$q^a(N)=aV$ $\lim_{N\to\infty}c_1^a(N)=\lim_{N\to\infty}c_2^a(N)=0$
Key images	Focus dominant	Pole dominant

in which $c_1(N)$ is found to be a constant and is independent of N. It indicates that the analytical solution by using the bipolar coordinates is the same as that of image method (special MFS) with only two sources as follows:

$$u(\xi,\eta)=\frac{V}{\sinh^{-1}\left(\frac{c}{a}\right)}\eta. \tag{27}$$

Fig. 16(a)–(c) show the potential contours by using the image method, the bipolar coordinates and the null-field BIEM [14], respectively. Good agreement of the three approaches is made.

Case 5: an eccentric annulus [12,16]

The problem sketch for an eccentric annulus is shown in Fig. 17 with $V_1=0$ and $V_2=1$. The radii of inner and outer circular holes are $a=1$ and $b=2.5$, respectively. The distance d between the two centers is equal to 1. This problem has been solved by using several approaches and a unified point of view by using the conformal mapping was provided in [13]. By putting successive images, the image solution can be obtained as below:

$$u(x)=\lim_{N\to\infty}\left\{q(N)\left[\ln r+\sum_{i=1}^{N}\left(-\ln|x-s_{2i-1}|+\ln|x-s_{2i}|\right)\right]+c_1(N)\ln|x-s_{c_1}|+c_2(N)\ln|x-s_{c_2}|+e(N)\right\}. \tag{28}$$

The coefficients of $q(N)$, $c_1(N), c_2(N)$ and $e(N)$ versus N are shown in Fig. 18. The analytical solution obtained by using the bipolar coordinates is given below:

$$u(\xi,\eta)=A\eta+B, \tag{29}$$

where

$$A=\frac{V_1-V_2}{\sinh^{-1}\left(\frac{c}{a}\right)-\sinh^{-1}\left(\frac{c}{b}\right)}, \tag{30}$$

$$B=V_1-\frac{V_1-V_2}{\sinh^{-1}\left(\frac{c}{a}\right)-\sinh^{-1}\left(\frac{c}{b}\right)}\sinh^{-1}\left(\frac{c}{a}\right). \tag{31}$$

It is also found that the solution derived by the image method and the MFS with only two sources are the same as the analytical solution derived by using bipolar coordinates. Fig. 19(a)–(c) show the potential contours by using the image method, the bipolar coordinates and the null-field BIEM, respectively. The frozen images happen to be the two focuses in the bipolar coordinates. It is found that the results of three approaches match well. In this case, the optimal number of sources in the MFS is only two and the two positions are found to be exactly located on the focuses in the bipolar coordinates. The image method in this case can be seen as an optimal and simple MFS.

For the 3D case, the successive strengths become smaller and the final strengths at the two frozen points approach zero for sufficiently large number of images. However, the 2D case is quite different, i.e., the strengths at the two centers are not $1/\ln(a)$ which satisfies the boundary condition (u=ln(a)/ln(a)=1). Only two singularities at the two focuses are required. In the cases of 4 and 5, we found the equivalence between the image solution and the analytical solution derived by using the separation of variables in the bipolar coordinates. Table 1 shows the comparison of the anti-symmetric problem between 2D and 3D cases. The image method can be seen as a simple MFS in the 2D case. For the five (2D and 3D) cases, all frozen images merge at the focuses. The present method can be also exactly extended to problems with Neumann BC or non constant boundary data. Since benchmark examples are not found, we do not provide more examples after five examples. Certainly, this approach can be applied to a general boundary problem once it can be mapped to a circular boundary.

4. Conclusions

In this paper, five solutions for the 2 and 3D BVPs were obtained by using the image method. For the 3D case, we have found the strengths of the two initial sources at the two centers that can be determined in advance to satisfy its own boundary condition. The strengths of successive images are then calculated and their values become smaller and smaller. The final strengths of frozen images approach zero for sufficiently large number of successive images. However, the finding in the 3D case can not be directly applied to the 2D case. Nonzero strengths at the frozen images are found and the initial strengths of sources at the centers are zero. The image method can provide optimal locations and specified weightings for the conventional MFS. The dimension of the matrix in the linear algebraic equation is at most four by four in the all examples. Agreement is made after comparing the image solution with those of the conventional MFS, the null-field BIEM, the analytical solutions by using the bipolar (2D) and the bispherical (3D) coordinates and the static result for limiting case of two-spheres radiation by using the null-field BIEM.

References

[1] P.M. Morse, H. Feshbach, Method of Theoretical Physics. Part I, McGraw-Hill, New York, 1953.
[2] J. Brunskog, Image solution for clamped finite beams, J. Sound Vib. 287 (2005) 1057–1064.
[3] M.D. Greenberg, Application of Green's Functions in Science and Engineering, Prentice-Hall, New Jersey, 1971.

[4] J.B. Keller, Progress and prospects in the theory of linear wave propagation, SIAM J. Numer. Anal. 21 (2) (1979) 229–245.
[5] J.B. Keller, The scope of the image method, Commun. Pure Appl. Math. 51 (1953) 505–512.
[6] R. Terras, Image methods for constructing Green's functions and eigenfunctions for domains with plane boundaries, J. Math. Phys. 21 (8) (1980) 2140–2153.
[7] M.S. Wu, H.Y. Wang, Solutions for edge dislocation in anisotropic film-substrate system by the image method, Math. Mech. Solids: MMS. 12 (2007) 183–212.
[8] T. Sometani, Image method for a dielectric plate and a point charge, Eur. J. Phys. 21 (2000) 549–554.
[9] J.T. Chen, Y.T. Lee, S.R. Yu, S.C. Shieh, Equivalence between Trefftz method and method of fundamental solution for the annular Green's function using the addition theorem and image concept, Eng. Anal. Bound. Elem. 33 (2009) 678–688.
[10] J.T. Chen, H.C. Shieh, J.J. Tsai, J.W. Lee, Equivalence between Trefftz method and method of fundamental solutions for the Green's function of concentric spheres using the addition theorem and image concept, in: C.A. Brebbia (Ed.), Mesh Reduction Methods BEM/MRM XXXI, WIT Press, 2009, pp.23–34.
[11] D.K. Cheng, Field and Wave Electromagnetics, Addison-Wesley, 1989.
[12] N.N. Lebedev, I.P. Skalskaya, Y.S. Uflyand, Worked Problems in Applied Mathematics, Dover Publications, New York, 1979.
[13] J.T. Chen, M.H. Tsai, C.S. Liu, Conformal mapping and bipolar coordinate for eccentric Laplace problems, Comput. Appl. Eng. Educ. 17 (3) (2009) 314–322.
[14] J.T. Chen, W.C. Shen, Null-field approach for Laplace problems with circular boundaries using degenerate kernels, Numer. Methods Partial Differ. Equ. 25 (1) (2009) 63–86.
[15] J.T. Chen, Y.T. Lee, Y.J. Lin, Analysis of multiple-spheres radiation and scattering problems by using the null-field integral equation approach, Appl. Acoust. (2010), in press.
[16] G.F. Carrier, C.E. Pearson, Partial Differential Equations Theory and Technique, Academic Press, New York, 1976.